

# Short Papers

## The Effect of Virtual Surface Stiffness on the Haptic Perception of Detail

Marcia K. O'Malley and Michael Goldfarb

**Abstract**—This brief presents a quantitative study of the effects of virtual surface stiffness in a simulated haptic environment on the haptic perception of detail. Specifically, the haptic perception of detail is characterized by identification, detection, and discrimination of round and square cross section ridges. Test results indicate that performance, measured as a percent correct score in the perception experiments, improves in a nonlinear fashion as the maximum level of virtual surface stiffness in the simulation increases. Further, test subjects appeared to reach a limit in their perception capabilities at maximum stiffness levels of 300 to 400 N/m, while the hardware was capable of 1000 N/m of maximum virtual surface stiffness. These results indicate that haptic interface hardware may be able to convey sufficient perceptual information to the user with relatively low levels of virtual surface stiffness.

**Index Terms**—Design specifications, haptic interface, haptic perception, virtual environment.

### I. INTRODUCTION

The proper design of any machine requires a well-defined set of performance specifications. Although much work has been accomplished in the field in general (see, for example, the surveys [1] and [2]), hardware specifications for haptic interfaces that relate machine parameters to human perceptual performance are notably absent. The absence of such specifications is most likely because haptic interface performance specifications must consider issues of human perception, which is complex in nature and difficult to assess quantitatively. With the recent introduction of several commercially oriented haptic devices and applications, the need for a set of specifications to guide the cost-optimal design of haptic devices is that much more pronounced.

Prior work published by the authors has characterized the effect of maximum force output on the ability of human subjects to perform perceptual tasks in a simulated environment [3]. Results showed that 3 to 4 N of maximum force feedback to the user was sufficient to achieve good performance in the perception tasks, while the hardware was capable of up to 10 N of continuous force feedback. Higher levels of force feedback did not produce better human performance in the tasks. This brief serves as a continuation of that prior work and investigates the effects varying virtual surface stiffness on human perception in simulated environments. Along with similar characterizations of other performance specifications, this work should help form a set of specifications from which a designer can effectively design a stylus-type haptic interface for a given application.

The vast majority of the research literature related to this topic has generally either focused on quantitative measures of human factors, measures of machine performance independent of human perception or the effects of software on the haptic perception of virtual environments.

Manuscript received February 25, 2003; revised Mar 22, 2003. This work was supported in part by NASA under Grant NGT-8-52859.

M. K. O'Malley is with the Department of Mechanical Engineering and Materials Science, Rice University, Houston, TX 77005 USA (e-mail: omalley@rice.edu).

M. Goldfarb is with the Department of Mechanical Engineering, Vanderbilt University, Nashville, TN 37235 USA (e-mail: goldfarb@vuse.vanderbilt.edu).

Digital Object Identifier 10.1109/TMECH.2004.828625

Regarding the first area, psychophysical experiments conducted by several research groups have quantified several haptic perception characteristics, such as pressure perception, position resolution, stiffness, force output range, and force output resolution (for example, [5]–[9]). Since these experiments did not involve haptic interface equipment, however, they were not able to create a direct link between machine performance and human perception during haptic task performance.

Within the second area of research, optimal machine performance has been characterized in the literature, yet these measures are typically disparate from human perceptual measures. When designing high-performance equipment, designers seek to build a device with characteristics such as high-force bandwidth, high-force dynamic range, and low-apparent mass [10], [11]. These are typically qualitative specifications, however, since the designers have little reference information regarding the quantitative effects of these machine parameters on the performance of humans with regard to perception in a haptically simulated environment. Several researchers have incorporated human sensory and motor capability as a prescription for design specifications of a haptic interface [12], [13]. Such measures are logical, though indirectly related to haptic perception and most likely quite conservative for common haptic tasks. Colgate and Brown offer qualitative suggestions for haptic machine design that are conducive to the stable simulation of high impedances [14]. Though simulation of a high impedance is a useful and logical performance objective for a haptic device, the objective is not directly based upon measurements of human perception.

Finally, researchers have studied the effects of software on the haptic perception of virtual environments (for example, [15]–[17]), yet these experiments did not address the relationships between haptic interface hardware design and haptic perception. This paper addresses the relationship between haptic interface hardware and human perception, and in particular measures the effects of varying virtual surface stiffness in a simulated environment on human perceptual capabilities in a haptic environment. Virtual surface stiffness is of interest as a machine parameter because hardware selections, including position sensors and computers, can limit achievable virtual surface stiffnesses. A good discussion of the relationship between hardware and achievable surface stiffness is given in [14].

Other than the authors' prior work that investigates the relationship between maximum force output and haptic perception, the only prior attempt (of which the authors are aware) to elucidate the relationship between haptic device design and human perception was the doctoral work of MacLean, which investigated the effects of machine sampling frequency and mechanical damping on human perception, and suggested "preliminary" design guidelines regarding these traits [4].

Unlike these prior works, this paper presents quantitative data on the effects of maximum virtual surface stiffness on the haptic display of detail in a stylus-type haptic device.

### II. METHODS

Three psychophysical concepts are generally used to quantify perception, namely detection, discrimination, and identification. Detection experiments, used to determine absolute detection thresholds, disclose the smallest parameter value that a subject can perceive. Unlike detection experiments, discrimination experiments reveal differential thresholds, or more specifically, the smallest perceivable difference in a parameter between a reference and a test object [18]. Finally, absolute identification paradigms measure a person's ability to categorize

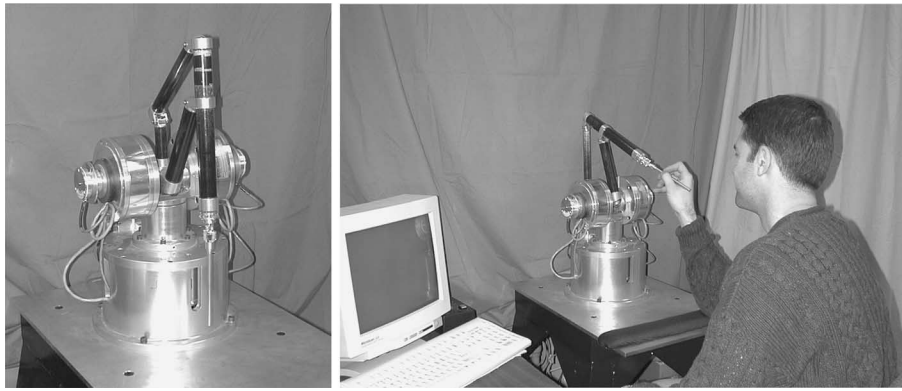


Fig. 1. Left, three-DOF manipulator used in perception experiments. Right, subject seated at the haptic interface for an experiment test session.

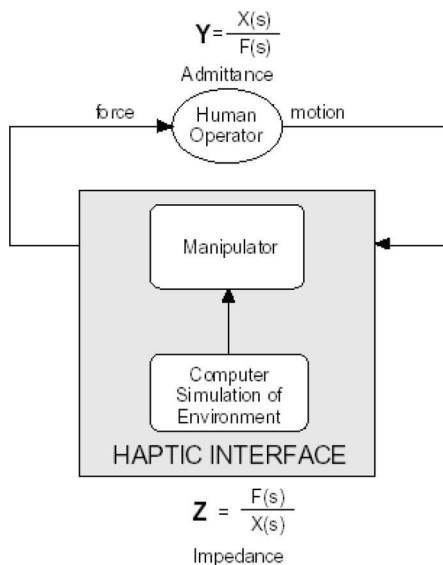


Fig. 2. Block diagram of the operator-interface feedback loop.

parameter values without providing explicit references. Collectively, when applied to haptic perception, these three perceptual measures serve to characterize the haptic display of detail.

### A. Apparatus

A three degree-of-freedom (DOF) manipulator, shown in Fig. 1, was designed to exhibit low inertia, minimal friction forces, zero backlash, and high link stiffness [19], which are physical characteristics generally known to facilitate high fidelity haptic simulations [10]. The manipulator is equipped with a pencil-type stylus device at the endpoint, and together with computer software designed to simulate virtual environments, was used to run a battery of experiments to test the effects of machine design on human perception through a haptic interface.

In the experiments described, the manipulator and haptic simulation were utilized as an impedance operator. A block diagram of the system is illustrated in Fig. 2. All simulations ran at a sampling frequency of 3000 Hz. System bandwidth is approximately 100 Hz, limited by first-order low-pass filters placed on each of the motor torque command signals to avoid excitation of structural resonance in the device. This particular direct-drive apparatus is capable of displaying constant forces of over 10 N in the spatial region of the haptically displayed ridges, and peak forces of roughly 40 N. The maximum achievable virtual surface stiffness with this hardware is 1000 N/m, limited by noise in the position signals. The dynamic characteristics and dynamic model of this haptic interface are described in detail in [19].

### B. Experimental Paradigms

Perception experiments were conducted for ridges of square and hemicylindrical cross sections, since both shapes can be characterized with a single parameter, namely the diameter (or radius) for the rounded ridges and the edge length for square ridges. These basic geometries can be easily combined to form more complex geometries.

The complete set of experiments consists of six sets of data. These are size identification of square and round cross section ridges (Experiments 1A and 1B), detection of square and round cross section ridges (Experiments 2A and 2B), and size discrimination of square and round cross section ridges (Experiments 3A and 3B).

During the training sessions and experiments, each subject sat in front of the haptic interface with the dominant hand holding the stylus and the nondominant hand typing responses on a keyboard, as pictured in Fig. 1. Keys for responses were selected to be a sufficient distance apart so as to avoid committing a slip and entering an undesired response. Nonsense responses (keystrokes other than those indicating possible responses) were ignored and the trial continued until a valid response was entered. The typical interval between sessions was one day, with a minimum interval of thirty minutes.

Since the objective of this work is to explore only the effects of machine parameters on haptic perception, no synthetically generated visual or audio feedback was included in the simulation. Though there were no measures taken to obstruct the subject's views of the haptic interface during testing, subjects were asked not to use static references (e.g., lining up the stylus tip with fixed points on the robot) to determine their responses. Subjects reported that the tasks relied heavily on their sense of touch and little on their sense of sight, despite the ability to see the motion of their hands. Even so, it is possible that the subjects' unobstructed vision may have impacted the results. Finally, there was no specific masking of the sound of the device, although the fans on the motor amplifiers tended to drown out any possible noises associated with the stylus interacting with the virtual environment.

### C. Subjects

In all, 16 male subjects between the ages of 21 and 35 participated in the experiments. Four subjects were left handed and twelve were right handed. Nine of the 16 subjects performed more than one of the perception tasks (identification, detection, and discrimination). Six test subjects participated in each experiment. These subjects were chosen from a pool of individuals with varying amounts of experience using a haptic interface. A cross section of subject types (dominant handedness and experience with haptic devices) was chosen for each of these experiments.

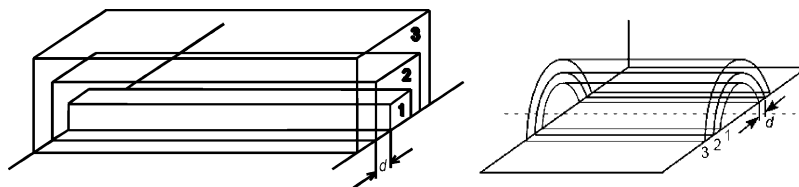


Fig. 3. Representation of square and round cross section ridges in three rendered sizes showing ridge size difference,  $d$ .

TABLE I  
K AND  $d$  VALUES FOR SIZE IDENTIFICATION TEST SESSIONS

Session Number	Stiffness ( $k$ ) Values (N/m)	$d$ (mm) Size Difference
1	50, 110, 220, 470, 1000	2.50
2	50, 110, 220, 470, 1000	5.00
3	50, 110, 220, 470, 1000	7.50
4	50, 110, 220, 470, 1000	10.00
5	50, 110, 220, 470, 1000	12.50

#### D. Procedures

1) *Experiment 1—Size Identification*: For Experiment 1, each subject was presented with five sessions of testing. A single session consisted of one set of ridge sizes and several randomly presented levels of virtual surface stiffness. The range of stiffnesses used in this experiment was logarithmically distributed across the range of achievable stiffnesses for this hardware, up to 1000 N/m. This maximum stiffness is limited by sensor noise in the position signals. Fig. 3 illustrates the three sizes of ridges used in the experiments. The radius of the smallest ridge was always 1 cm. The medium and large sizes were generated by adding a constant  $d$ , the ridge size difference, to this radius. Recall that for square ridges, the “radius” corresponds to half the edge length. The minimum stiffness tested was 50 N/m. Below this stiffness, the authors could not feel the simulated surface. Test values were then selected in the range of 50 to 1000 N/m. The range of object sizes used in the final sets of experiments was based on previous runs of Experiment 1 with maximum force output as the machine parameter of interest [3]. Table I shows ridge size differences and stiffness values for the size identification experiments.

A training session occurred before each testing session, allowing the test subject to learn the three ridge sizes for that particular session. Instructions indicated that training should cease when the subject felt comfortable with the sizes and confident that she or he could classify ridges by size to the best of their ability.

During experimentation, stiffness values were assigned on a trial-by-trial basis, and damping values were calculated to maintain a constant ratio of damping to stiffness of 0.1. The subjects were instructed to classify the randomly presented ridges into one of the three size categories, and responses were tabulated so that percent correct scores for each test condition could be calculated after testing was completed. Subjects entered the number of the size corresponding to their response on an adjacent keyboard with the nondominant hand.

2) *Experiment 2—Object Detection*: Ridges of either square or round cross section were presented at random positions between a simulated stiff front wall and a simulated stiff back wall approximately 10-cm apart. The stimuli were oriented horizontally and perpendicular to the subject’s midline. For the detection tests, stiffnesses below 100 N/m were not tested because subjects reported that they could not feel anything in the simulated environment for such low values of  $k$ . Ridge sizes were varied from a radius (or half of edge length for square ridges) of zero to 5.0 mm for these tests. Refer to Table II for all values used in detection experiments.

Two test sessions were performed and subjects were allowed to practice the experiment with correct-answer feedback in a maximum stiff-

TABLE II  
STIFFNESSES AND RIDGE SIZES USED IN DETECTION EXPERIMENTS

Stiffness ( $k$ ) Values (N/m)	100	220	460	1000				
$d$ (mm) Sizes	0	0.25	0.5	0.75	1	1.25	2.5	5

ness session prior to testing. Each session consisted of 256 trials, where each combination of stiffness and object size was presented eight times. The combinations tested in each session were identical; however the order of presentation differed due to the random automation of the experiments. Percent correct scores were tabulated for the sixteen responses given over the span of the two sessions for each stiffness-size pair. The range of size differences tabulated for each value of  $k$  for the object detection data was 0.5 to 2.5 mm. Subjects typed “s” for square, “r” for round, or “n” for none. Yes responses were recorded for both the “s” and “r” responses.

3) *Experiment 3—Size Discrimination*: The final experiment for the evaluation of varying stiffness on haptic perception was size discrimination. Square and round ridges were presented in separate groups. For either test, ridges were displayed side-by-side along a common centerline in the haptic interface workspace. The stimuli were oriented horizontally and perpendicular to the subject’s midline. The testing environment is shown in Fig. 4. Subjects typed their responses (“1” for left, “3” for right, or “0” for same) on the number pad of an adjacent keyboard.

For each session, one of the two ridges was randomly defined with a reference radius of 1.0 cm. To set the discrimination size  $d$ , one of six sizes was selected at random and added to a radius of 1.0 cm. Six ridge discrimination sizes were used (0, 1.25, 2.50, 5.00, 7.50, and 10.00 mm) with four stiffness levels (110, 220, 470, and 1000 N/m). Seven presentations of each combination comprised one session, for a total of 168 trials per session. Two complete sessions were conducted for each test subject. Again, a training session was allowed prior to each test session with correct answer feedback and maximum stiffness. The experiment was not forced choice. Responses were recorded and percent correct scores were calculated at the end of the experiment.

### III. RESULTS AND DISCUSSION

Results of all experiments are presented here. To determine the confidence interval for each experiment, three-way analysis of variance (ANOVA) tests were performed for all perception experiments. ANOVA results are shown in Table III, with significant results highlighted by shading. Two treatments, the levels of stiffness and the feature sizes or size differences, are used, and results are blocked on subjects.

#### A. Experiment 1—Size Identification

Experiment 1 studied the ability of subjects to classify objects presented one at a time by size. Square ridge testing was conducted in Experiment 1A, while round ridge testing was conducted in Experiment 1B. Percent correct scores were tabulated for each stiffness level—size difference pair presented in the experiment sessions, and scores were

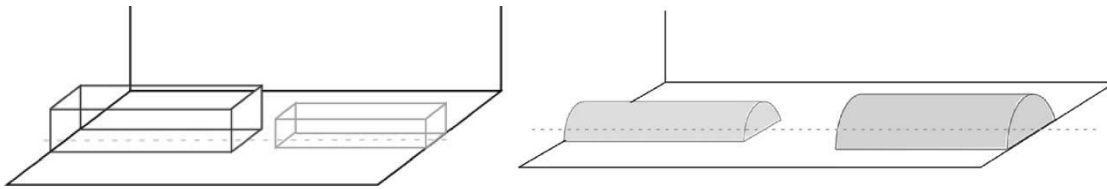


Fig. 4. Square and round cross section ridges in the size discrimination testing environment.

TABLE III  
ANOVA RESULTS FOR ALL PERCEPTION EXPERIMENTS

Experiment	Treatment #1 Ridge size or <i>d</i>	Treatment #2 k level	Block Subjects	#1-#2 Interaction	#1-Block Interaction	#2-Block Interaction
1A	Square ridge size id F(4,80) = 165.26 P = 0.0001	F(4, 80) = 54.46 P = 0.0001	F(5, 80) = 64.91 P = 0.0001	F(16,80) = 0.63 P = 0.8492	F(20, 80) = 4.27 P = 0.0001	F(20, 80) = 4.2 P = 0.0001
1B	Round ridge size id F(4,80) = 76.79 P = 0.0001	F(4, 80) = 76.79 P = 0.0001	F(5, 80) = 48.19 P = 0.0001	F(16,80) = 1.79 P = 0.0468	F(20, 80) = 4.15 P = 0.0001	F(20, 80) = 2.7 P = 0.0009
2A	Square ridge detection F(4,60) = 8.68 P = 0.0001	F(3, 60) = 10.49 P = 0.0001	F(5, 60) = 14.22 P = 0.0001	F(12,60) = 2.64 P = 0.0067	F(20, 60) = 3.4 P = 0.0001	F(15, 60) = 4.73 P = 0.0001
2B	Round ridge detection F(4,60) = 4.58 P = 0.0027	F(3, 60) = 12.01 P = 0.0001	F(5, 60) = 13.47 P = 0.0001	F(12,60) = 2.17 P = 0.025	F(20, 60) = 2.21 P = 0.0097	F(15, 60) = 7.03 P = 0.0001
3A	Square size dis- crim F(4,60) = 184.11 P = 0.0001	F(3, 60) = 1.54 P = 0.2127	F(5, 60) = 12.93 P = 0.0001	F(12,60) = 0.9 P = 0.5553	F(20, 60) = 3.36 P = 0.0001	F(15, 60) = 1.23 P = 0.2751
3B	Round size discrim F(4,60) = 193.62 P = 0.0001	F(3, 60) = 1.36 P = 0.2622	F(5, 60) = 96.54 P = 0.0001	F(12,60) = 1.29 P = 0.2493	F(20, 60) = 5.33 P = 0.0001	F(15, 60) = 1.17 P = 0.3162

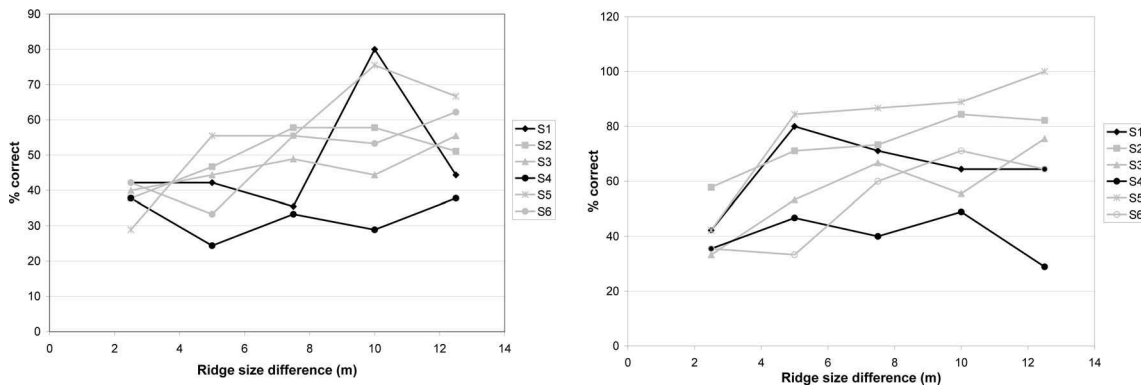


Fig. 5. Subjects-sizes interactions for 50 (left) and 110 (right) N/m wall stiffness [note the different trends for S1 (increasing/decreasing) and S4 (stagnant/decreasing)].

averaged across all test subjects. Then, exponential curves were fit to these averaged data points according to the methods described in [3]. The effects of both treatments (size difference and stiffness) and subjects were significant. Significant interactions occurred for interactions involving subjects and one of the treatments. The interaction plots indicate that the interactions are mainly attributable to nonparallel trends in performance by one subject. A representative interaction plot is shown in Fig. 5.

The exponential curves corresponding to average percent correct scores for all subjects were plotted versus each ridge size difference set for all stiffness levels. The results for Experiment 1A are pictured in Fig. 6. The graph in Fig. 7 shows system stiffness levels versus difference in ridge radius for Experiment 1A, and was compiled using methods described in [3]. Fig. 7 presents the 90% correct crossover points for each stiffness level curve in Fig. 6, showing the minimum size difference necessary for an average of 90% correct performance in the size identification task. Then, the plus and minus standard deviation curves are plotted, similar to Fig. 6, and their 90% crossover points are determined. These points are presented as the +/- standard deviation curves and represent the performance band for each experiment. This performance graph shows that as stiffness of virtual walls increases, performance of the size identification task improves. This holds until the stiffness reaches about 300 to 400 N/m, beyond which

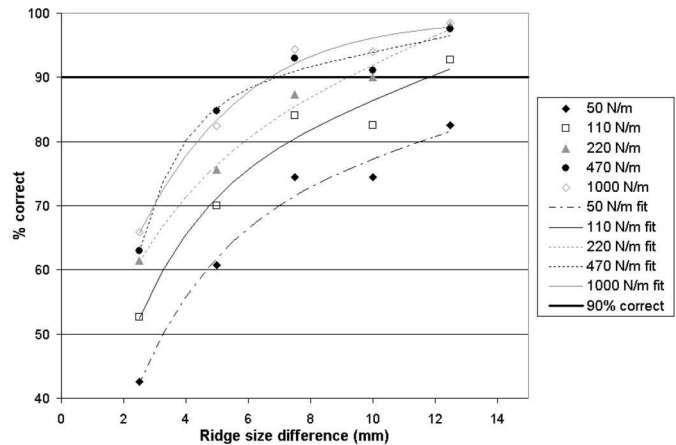


Fig. 6. Summary plot of Experiment 1A results (square ridge size identification) for all stiffness levels.

significant gains in performance are not seen. Once this stiffness level is reached, the average user is able to correctly identify size differences of 7 mm with 90% accuracy. The maximum bound is not calculable for

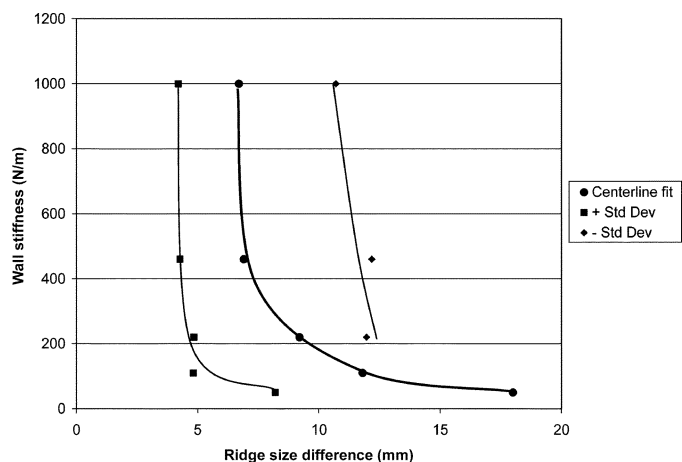


Fig. 7. Wall stiffness versus ridge "radius" size difference ( $d$ ) performance band for Experiment 1A (square ridge size identification).

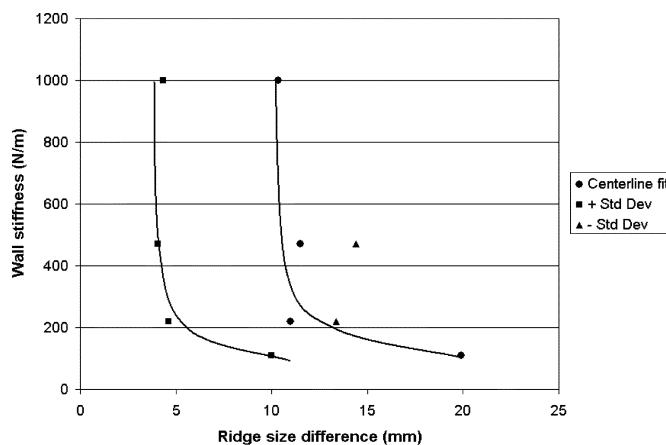


Fig. 9. Wall stiffness versus ridge radius size difference ( $d$ ) performance band for Experiment 1B (round cross section size identification).

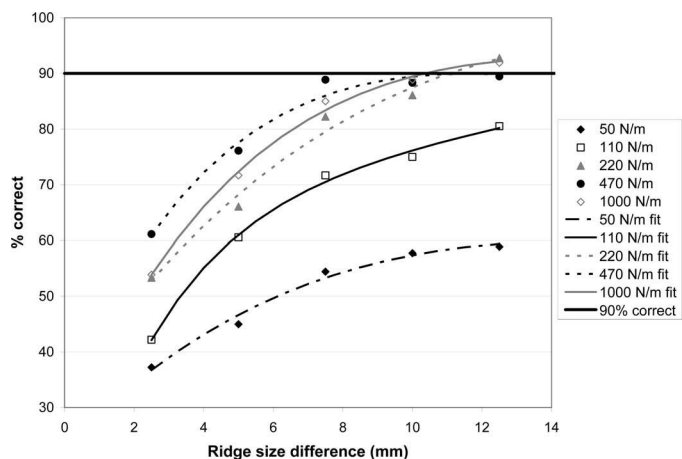


Fig. 8. Summary plot of Experiment 1B results (round ridge size identification) for all stiffness levels (subjects 1 and 4 excluded).

stiffnesses of 50 and 110 N/m because these standard deviation bands did not reach the 90% correct line.

A similar analysis procedure was followed when recording and compiling data for the size identification tasks involving objects with semi-circular cross sections. As with Experiment 1A, the effects of both treatments (size difference and stiffness) and subjects were significant. Upon examination of ANOVA interaction plots shown in Fig. 5, however, subjects 1 and 4 were found to have nonparallel performance when compared to the other subjects, and thus their data was considered aberrant and were not included in the summary plot. The summary plot of results for various stiffnesses, excluding subjects 1 and 4, is shown in Fig. 8. The performance band plot of Fig. 9 was similarly constructed without data from subjects 1 or 4. No plus standard deviation trend line is shown because only two data points were generated from the 90% crossover graphs. The Experiment 1B summary results indicate that, as seen in Experiment 1A, performance in the size identification task improves as stiffness increases up to approximately 300 N/m. At higher stiffnesses, additional improvements in performance are minimal. According to the summary graph, an average subject could identify size differences of 10 mm at stiffnesses above 300 N/m.

### B. Experiment 2—Object Detection

In Experiment 2, the effects of both the treatments and the subjects were significant, as seen in Table III. Significance of interactions is

noted for the detection experiments. This finding supports the conclusions made in [3] regarding results in detection experiments. There it was stated that the geometry of the ridges in the detection tests affected force output more than the variation of the machine parameter. Because these ridges are small, and because the output force command is proportional to the depth of penetration into the simulated ridge, the user has pushed through the simulated object before high forces are generated. This relationship explains the interaction between ridge size and stiffness level.

Percent correct scores for the detection of square (Experiment 2A) and round (Experiment 2B) features were tallied versus the size of the objects to be detected, and are shown in the summary plots of Fig. 10 (Experiment 2A and Experiment 2B). For Experiments 2A and 2B, all sizes were correctly detected with over 90% accuracy for stiffnesses above 220 N/m. Smaller ridges could not be simulated due to geometric limitations of the virtual wall model. Upon close inspection of Fig. 10, performance seems to be the same for stiffnesses of 460 and 1000 N/m, with performance at 220 N/m just slightly lower. Therefore, it could be argued that a minimum stiffness of 220 N/m will result in maximum performance for the object detection experiments.

### C. Experiment 3—Size Discrimination

Size discrimination experiments were performed in two groups, one for each shape of ridge. It should be noted that the ANOVA for Experiments 3A and 3B indicates that variations in subject scores are not attributable to changing virtual surface stiffness with a high level of confidence. The effects of size difference and subject were significant for both Experiments 3A and 3B. Significant interactions occurred in both cases for interactions involving subjects and one of the treatments (stiffness level). As before, the interaction plots indicate that these are mainly attributable to nonparallel trends in performance by one subject.

A performance band plot of the results of Experiment 3A (square ridges) is presented in Fig. 11. These results, compiled in the same manner as those for the detection and identification experiments, indicate that as stiffness increases, performance in the size discrimination task increases up to stiffnesses of 300 to 400 N/m. Above this level, the average subject is able to discriminate size differences of 4 mm (for square ridges) with 90% accuracy. Results of Experiment 3B, shown in Fig. 12, were comparable to those of Experiment 3A, though the minimum size difference was somewhat larger (i.e., approximately 5 mm rather than 4), indicating that ridge shape only weakly affects performance for the size discrimination task. Performance gains were not significant for stiffnesses above 400 N/m. At and above this stiffness

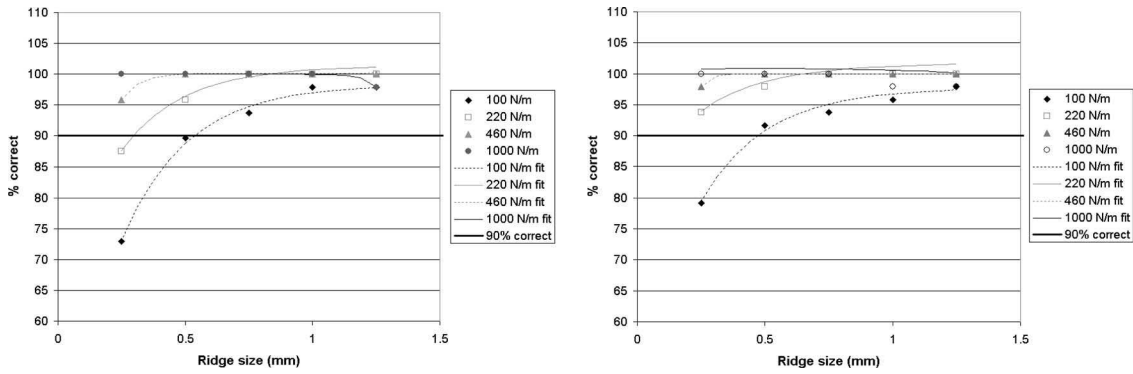


Fig. 10. (left) Summary plot of Experiment 2A results (square ridge detection) for all stiffness levels. (right) Summary plot of Experiment 2B results (round ridge detection) for all stiffness levels.

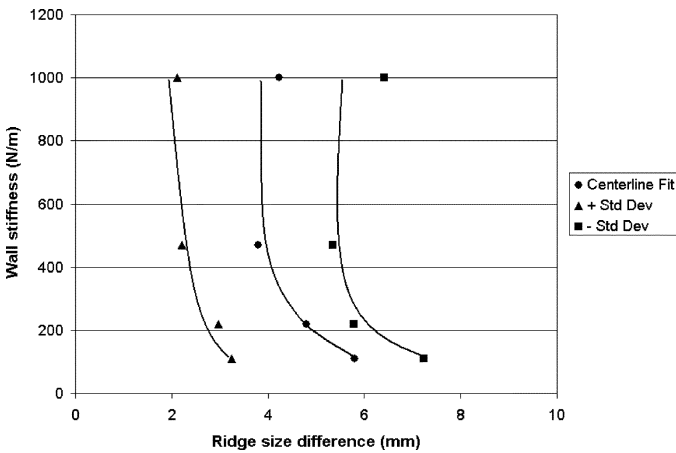


Fig. 11. Experiment 3A (size discrimination with square ridges) performance band. Stiffness versus ridge size difference for 90% accuracy.

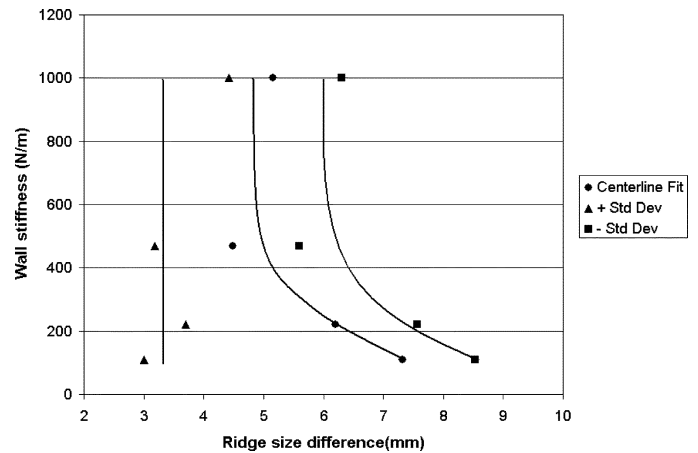


Fig. 12. Experiment 3B (size discrimination with round ridges) performance band. Stiffness versus ridge size difference for 90% accuracy.

level, the average subject could discriminate size differences of 5 mm with 90% accuracy.

IV. CONCLUSIONS

Identification, detection, and discrimination tests were performed to characterize the effect of virtual surface stiffness on haptic perception of detail in a simulated environment. For haptic simulation in a stylus-type interface, the following relationships were observed.

- Stiffnesses above 400 N/m do not provide any significant improvements in performance (defined at 90% accuracy) for size identification tasks with ridges of square and round cross sections.
- Stiffnesses above 220 N/m may not provide any significant improvements in performance (defined at 90% accuracy) for object detection tasks with ridges of square and round cross sections;
- Stiffnesses above 400 N/m do not provide any significant improvements in performance (defined at 90% accuracy) for size discrimination tasks with ridges of square and round cross sections; however, ANOVA analysis indicates that variations in results are not attributable to varying simulated surface stiffness with a sufficient level of confidence.

These observations indicate that haptic interface hardware may be capable of conveying significant perceptual information to the user at low to moderate levels of simulated surface stiffness for gross stylus-type perceptual tasks.

REFERENCES

- [1] G. C. Burdea, *Force and Touch Feedback for Virtual Reality*. New York: Wiley, 1996.
- [2] M. A. Srinivasan, "Haptic interfaces," in *Virtual Reality: Scientific and Technological Challenges*, N. I. Durlach and A. S. Mavor, Eds. Washington, DC: Nat. Res. Council, Nat. Academy, 1994, ch. 4.
- [3] M. K. O'Malley and M. Goldfarb, "The effect of force saturation on the haptic perception of detail," *IEEE/ASME Trans. Mechatron.*, vol. 7, pp. 280–288, Aug. 2002.
- [4] K. E. MacLean, "Emulation of haptic feedback for manual interfaces," Ph.D. dissertation, Mass. Inst. Technol., Cambridge, MA, 1996.
- [5] G. L. Beauregard, M. A. Srinivasan, and N. I. Durlach, "The manual resolution of viscosity and mass," in *Proc. ASME Dynamic Systems Control Division*, 1995, pp. 657–662.
- [6] L. A. Jones, "Matching forces: Constant errors and differential thresholds," *Perception Psychophysics*, vol. 18, no. 5, pp. 681–687, 1989.
- [7] K. D. Pang, H. A. Tan, and N. I. Durlach, "Manual discrimination of force using active finger motion," *Perception Psychophysics*, vol. 49, no. 6, pp. 531–540, 1991.
- [8] H. Z. Tan, M. A. Srinivasan, B. Eberman, and B. Cheng, "Human factors for the design of force-reflecting haptic interfaces," in *Proc. ASME Dynamic Systems Control Division*, 1994, pp. 353–359.
- [9] N. I. Durlach, L. A. Delhome, A. Wong, W. Y. Ko, W. M. Rabinowitz, and J. Hollerbach, "Manual discrimination and identification of length by the finger-span method," *Perception and Psychophysics*, vol. 46, pp. 29–38, 1989.
- [10] R. Ellis, O. Ismael, and M. Lipsett, "Design and evaluation of a high-performance prototype planar haptic interface," *Adv. Robotics, Mechatron., Haptic Interfaces*, pp. 55–64, 1993.
- [11] T. L. Brooks, "Telerobotic response requirements," in *Proc. IEEE Conf. Systems, Man, Cybernetics*, 1990, pp. 113–120.

- [12] C. D. Lee, D. A. Lawrence, and L. Y. Pao, "A high-bandwidth force-controlled haptic interface," in *Proc. ASME Dynamic Systems and Control Division*, 2000, pp. 1299–1308.
- [13] B. D. Adelstein and M. J. Rosen, "Design and implementation of a force reflecting manipulandum for manual control research," in *Advances in Robotics*, H. Kazerooni, Ed. New York: ASME, 1992, pp. 1–12.
- [14] J. E. Colgate and J. M. Brown, "Factors affecting the Z-width of a haptic display," in *Proc. IEEE Int. Conf. Robotics and Automation*, 1994, pp. 3205–3210.
- [15] P. A. Millman and J. E. Colgate, "Effects of nonuniform environment damping on haptic perception and performance of aimed movements," in *Proc ASME Dynamic System Control Division*, 1995, pp. 703–711.
- [16] L. B. Rosenberg and B. D. Adelstein, "Perceptual decomposition of virtual haptic surfaces," in *Proc. IEEE Symp. Research Frontiers Virtual Reality*, San Jose, CA, Oct. 1993, pp. 46–53.
- [17] H. B. Morgenbesser and M. A. Srinivasan, "Force shading for haptic shape perception," in *Proc. ASME Dynamic Systems and Control Division*, 1996, pp. 407–412.
- [18] G. A. Gescheider, *Psychophysics: Method, Theory, and Application*, 2nd ed. Hillsdale, New Jersey: Lawrence Erlbaum Associates, 1985.
- [19] C. M. Perry, "Design of a High Performance Robot for Use in Haptic Interface and Force Feedback Research," Master's thesis, Dept. of Mech. Eng., Vanderbilt Univ., Nashville, TN, 1997.

## Real-Time Slip-Based Estimation of Maximum Tire-Road Friction Coefficient

Chankyu Lee, Karl Hedrick, and Kyongsu Yi

**Abstract**—This paper presents a real-time maximum tire-road friction coefficient estimation method and field test results. The estimator is based on the relationship between the wheel slip ratio and the friction coefficient. An effective tire radius observer and a tire normal force observer have been designed for the computation of the slip ratio from wheel speed and vehicle speed measurements. The effective tire radius observer has been used so that the proposed method works for all driving situations. A tractive force estimator, a brake gain estimator, and a normal force observer have been used for the estimation of the friction coefficient. The proposed estimation method for the maximum tire-road friction coefficient has been implemented using a fifth wheel and typical vehicle sensors such as engine speed, carrier speed, throttle position, and brake pressure sensors.

**Index Terms**—Brake gain, friction coefficient, recursive least square method, slip ratio, tractive force.

### I. INTRODUCTION

Driver assistance or machine-controlled systems including Automated Highway System, Adaptive Cruise Control, and Stop-and-Go Cruise Control System require proper safety and vehicle control performance. From this point of view, knowing the maximum friction coefficient ( $\mu_{MAX}$ ) is advantageous in the area of effective vehicle

control and safety because the maximum braking performance is related with the maximum tire-road friction coefficient shown in (1)

$$\begin{aligned} |a|_{MAX} &= \text{MAX} \left| \frac{F_t}{m} \right| = \text{MAX} |\mu \cdot F_N| \\ &= \text{MAX} \left| \mu \cdot m \cdot \frac{g}{m} \right| = \mu_{MAX} g. \end{aligned} \quad (1)$$

$F_t$ ,  $F_N$ ,  $m$  are tire tractive force, normal force on tire, and vehicle mass, respectively. Due to the importance of  $\mu_{MAX}$ , many researchers have accomplished obtaining  $\mu_{MAX}$  using various methods [1]–[15]. Tire-road friction estimation research can be divided into "cause-based" and "effect-based" approaches. Cause-based approaches try to detect factors that affect the friction coefficient, and then predict  $\mu_{MAX}$  using a tire model or a certain analytical theory. Although experimental results often show a high accuracy, this method requires special sensors such as lubricant or optical sensors. Also, this method requires accurate tire models for a certain road condition as well as training software [1]–[3]. Effect-based research focused on the effects that are generated by friction. The effects are shown in the tire as an acoustic characteristic, tire-tread deformation and wheel slip. The acoustic method estimates  $\mu_{MAX}$  using tire sound, but the complexity of the tire nature noise makes it difficult to estimate  $\mu_{MAX}$  [1]–[3]. The method of observing tire deformation uses a certain sensor that is fixed to the inner surface of the tire. But this method needs a specially equipped sensor and lacks an accurate relationship between tire deformation and  $\mu_{MAX}$  [1]–[3]. The last method in the effect-based approach is the slip-based approach, which uses the wheel slip ratio and friction coefficient data. Because more slip at a given tire force would indicate a more slippery road, observing the correlation between slip and friction coefficient can give  $\mu_{MAX}$  information [4]–[8], [11], [12]. However, most research focuses on normal driving, acceleration and braking separately. Also some research requires special sensors and an accurate tire model, which depends on the road condition. However, because  $\mu_{MAX}$  changes not only through road conditions but also through tire conditions, an experiment-based real-time  $\mu_{MAX}$  estimator using typical vehicle sensors under different driving conditions is interesting.

### II. METHOD OVERVIEW

In this brief, slip ratio is defined by wheel radius ( $r$ ), wheel angular velocity ( $\omega$ ), and vehicle speed ( $v$ ) as shown in (2). Also, the friction coefficient is defined by the normal force,  $F_N$ , divided by the longitudinal tire force,  $F_t$  as shown in (3). Because we considered just longitudinal motion, the lateral tire force is neglected

$$s = \frac{r\omega - v}{\max(r\omega, v)} \quad (2)$$

$$\mu = \frac{F_t}{F_N}. \quad (3)$$

With the slip and friction coefficient definitions above, the relationship of these factors is shown in Fig. 1. This well-known relationship is called the "magic formula" [16]. In a certain small slip range, the correlation between  $s$  and  $\mu$  has a linear characteristic. We concentrate on this linear characteristic called the slip slope. Because slip slope and  $\mu_{MAX}$  change depending on road condition (dry, wet, snowy, or icy), road type (asphalt, concrete, gravel, or earth), tire type (carcass or radial ply), tread type, and tread depth, we can infer  $\mu_{MAX}$  from observing the slip slope. Fig. 2 shows the schematic of the maximum friction coefficient estimator, which is activated under cruising, acceleration or

Manuscript received December 9, 2002; revised September 18, 2003; October 6, 2003. This work was supported by the Naval Research Laboratory (NRL) under Project M103020000903J000000610 and the California PATH.

C. Lee was with the Department of Automotive Engineering, Hanyang University, Seoul, Korea. He is now with the Hyundai Motor Company, Seoul, Korea (e-mail: chankyulee@hotmail.com).

K. Hedrick is with the Department of Mechanical Engineering, University of California, Berkeley, CA 94720 USA (e-mail: khedrick@me.berkeley.edu).

K. Yi is with the School of Mechanical Engineering, Hanyang University, Seoul, Korea (e-mail: kyongsu@hanyang.ac.kr).

Digital Object Identifier 10.1109/TMECH.2004.828622